Adaptive Fractional Order Sliding Mode Speed and Current Control for Switched Reluctance Motor

Ashraf Abdalla Hagras

Egyptian Atomic Energy Authority (EAEA), Abo Zaabal, 13759 Cairo, Egypt; ashraf.hagras@eaea.org.eg

Abstract: This paper applies a Fractional Order Sliding Mode Control (FOSMC) to the two loops speed (the outer loop) and current (the inner loop), for Switched Reluctance Motor (SRM). This approach proposes a new, simple and fast switching control law for the Fractional Order Sliding Mode Control (FOSMC), characterized by its simplicity of design, flexibility of control and adaptive capability. The proposed controller is based on nonsingular terminal SM surface. The stability of the proposed approach was analyzed and guaranteed, using the Lypunov stability theory. This new scheme achieved minimum torque and speed ripples. Simulation results using MATLAB/SIMULINK validated the improved performance of the proposed approach against parameters variations, external disturbances and measurement noise, by comparing it with PI, Neural Network Controller (NNC), Hysteresis Controller (HC) and conventional Sliding Mode Controllers (SMC).

Keywords: Fractional order SMC; Speed Control; Current Control; Switched Reluctance Motor (SRM); Neural Network Controller (NNC)

1 Introduction

Switched Reluctance Motor (SRM) is a low-cost machine because it has neither winding nor permanent magnets in the rotor nor brushes nor commutators. Also, it is reliable because their phases can be feed independently and connected in series with the DC power supply. This makes its drive robust compared to the other electrical machines drives. Besides, its drive is simple because of its unidirectional current. However, it has high coupling and nonlinearities between the current and the position [10]. Torque ripples and high starting torque are other obstacles. Therefore, PI can't overcome these difficulties and advanced control methodologies were proposed to overcome these disadvantages [1, 2, 26, 27]. Speed control of the motor was carried using PI but its gains were tuned using bat algorithm [3] or using ant-colony optimization algorithm [4] or using Particle Swarm Optimization (PSO) and the Zeigler Nicholas method [5, 8] to improve the

performance of the controller. But in [6] speed control using PID and current sharing method parameters need to optimize its gains using three methods of evolutionary computation methods like PSO. In [7] the authors confirmed the improved performance of speed control by the ASK fuzzy control using on-line tuning and comparing it with fuzzy and PI controllers. The authors of [8] designed vector control scheme using PI added to feed-forward and decoupling controllers for SRM to overcome the problems of the torque controller. Therefore, PI is known with its difficult parameters tuning in addition to its inherent disadvantages like slow transient response and steady state error [9]. But, the proposed method in our paper avoided these difficulties with minimum number of parameters.

Intelligent methods like fuzzy and neural network were proposed to control the speed loop. As shown in [11, 12], the fuzzy controller used another strategy to improve its performance. In [13], speed control by modified fuzzy controller was used to decrease the rise time and the overshoot of the speed response. This controller includes two fuzzy controllers and switches between them. In [14], the RBF Neural Network (NN) controller added to another RBF NN for on line training controls the speed to overcome the nonlinearities and provide fast speed response. But in [15, 16], the RBF NN and hermite NN decreases the model errors resulting from parameters uncertainties for fast terminal and super twisting second order sliding mode speed control respectively. While [17] applied a Supervisor Hybrid Recurrent Fuzzy Neural Network (SHRFNN) controller to the speed control loop to reduce the torque ripples. Therefore, the proposed strategy avoided using more than one strategy as used in the above intelligent methods using simple switching control law which provided more flexibility and more degrees of freedom.

Therefore, advanced control techniques like Sliding Mode Control (SMC) were employed to achieve fast response and robust performance against the nonlinearities and coupling of the rotor position, current and the self-inductance. At the same time, this technique was developed to overcome its disadvantages like slow convergence, the chattering effect and the conventional difficulties of PI. Therefore, new Fast Terminal Sliding Mode Controller (FTSMC) was combined with fuzzy logic [18] to control the speed and reduce the torque ripples of SRM. A current and flux sharing method is designed for SRM by employing Proportional and Derivative (PD) controller and Adaptive Linear Element (Adaline) with sliding mode learning algorithm to control the speed loop of SRM [19]. In [20], a new reaching law was designed for the speed loop of adaptive terminal SMC of direct instantaneous torque to decrease the torque ripples and speed the speed and torque response. Ref. [21] designed new reaching law for SMC of speed control in addition to anti-disturbance SMC to obtain anti-disturbance speed control strategy. As shown in the previous literature, SMC types needed other techniques to improve its performance which add complexity to the controller and add to the computational overhead of the processor which were avoided by the proposed method [22, 23].

The main contributions of this paper are as follows:

1) Novel application of fractional order sliding mode control to the speed and current loop of SRM simultaneously.
2) The speed and torque ripples were minimized, the chattering phenomenon was eliminated and the convergence time was reduced.
3) FOSMC doesn't need the process model or its parameters and consequently, the proposed strategy avoided heavy and multi parameters tuning.

This paper was organized as follows: Section 1 presents the introduction and literature review. Section 2 shows the mathematical modeling of SRM and the controllers. Section 3 displays the design and the stability proof of the proposed technique. Simulation results were shown in Section 4 and the conclusions were drawn in Section 5.

2 Mathematical Modeling of Switched Reluctance Motor (SRM)

The number of poles of SRM determines the type of the motor and controls the structure of the motor. Each phase is excited independently from the DC power supply. Each phase should be excited in the magnetization period where the two switches S1 and S2 are on. After that the magnetization period completes with the freewheeling mode when S2 is off and the current passes through S1 and D1. The demagnetization period starts when S1 and S2 are turned off and the current is reversed to the DC power supply through D1 and D2. Therefore, the current should be zero before the aligned position.

Therefore, selection of turn on θ_{on} and turn off θ_{off} angles is an important factor to improve the performance of SRM drive. They should be selected after the unaligned position θ_u and before the aligned position θ_a. The motor will provide positive torque when its winding current is turned off before the aligned position θa. In this work, they were selected as 45º and 90º [13]. Figure 1 shows the block diagram of the proposed system.

The mathematical modeling of SRM can be expressed by the following equations:

$$V_n = R_n i_n + \frac{d\lambda(\theta, i_n)}{dt} = R_n i_n + \left(\frac{\partial\lambda(\theta, i_n)}{\partial i_k}\right)\left(\frac{di_n}{dt}\right) + \frac{\partial\lambda(\theta, i_n)}{\partial\theta}.\omega \tag{1}$$

$$T_e = J\frac{d\omega}{dt} + B\omega + T_L \tag{2}$$

$$\theta = \frac{d\omega}{dt} \tag{3}$$

Where n: the number of phase, θ is the rotor position, ω is the rotor speed, T_L the load torque, T_e is the total torque of the motor, B is the viscous friction coefficient and J is the moment of inertia of the motor.

$$\partial\lambda(\theta,i_n)=L(\theta,i_n).i_n \tag{4}$$

$$T_e(\theta,i_n)=\sum T_n(\theta,i_n)=\left[\frac{\partial W_c(\theta,i_n)}{\partial\theta}\right]_{i_n=cons.}, \quad W_c(\theta,i_n)=\int_0^{i_n}\lambda(\theta,i_n)di_n$$

Where L_n, T_n, W_c and i_n are the inductance, torque, co-energy and the current of the nth phase, respectively

In the linear region of the relationship between the position, the phase current and the self-inductance in low current SRM, the inductance and the flux can be computed as follows:

$$T_e(\theta,i_n)=\frac{1}{2}i_n^2\frac{dL_n(\theta)}{d\theta} \tag{5}$$

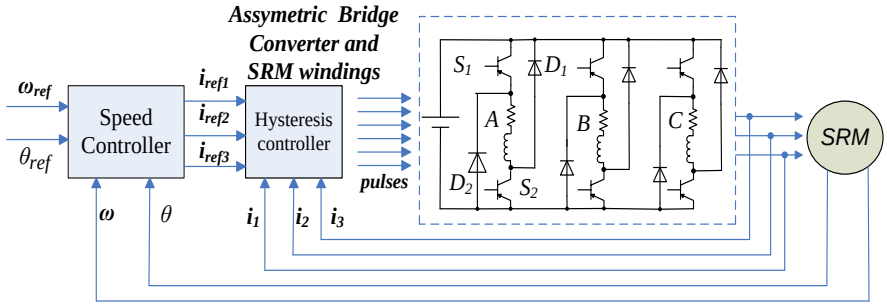

Figure 1
The Block Diagram of the Proposed System

3 Speed and Current Controllers Design

The control system of the SRM drive includes two main loops; the outer Speed Loop (SL) and the inner Current Loop (CL) as shown in Figure 1. The mechanical equation (2) controls the speed loop. Since the mechanical motor parameters; the inertia and the friction coefficients affect this equation and have larger time constant compared to the electrical parameters (the stator inductance and resistance) and its time constant which control the current loop, the speed loop has larger effect compared to current loop. Therefore, the actual speed, phase current and position should be measured to be compared to the reference and processing the error in each loop controller.

3.1 Speed Control

3.1.1 PI Controller

In order to control the speed of SRM, the error of the reference speed and the actual speed should be processed through the PI controller. The output of the controller is the reference torque after normalizing it.

3.1.2 Neural Network Controller (NNC)

The NNC is composed of a pattern set, an off-line learning algorithm with back propagation and a NN network. The NN is trained off-line using the Levenberg–Marquardt training algorithm with the ANN toolbox under MATLAB. For the off-line learning, a pattern set is realized using dynamic signal analysis of the PI controller. The input–output samples, obtained using simulations in Matlab /Simulink were used for off-line training. The pattern set is a look up table that consists of $e_w(l)$, $t(l)$ and $\Delta I^*(l)$. l is number of samples in the pattern set (l = 1,. . ., 64). The look up table is used in off-line learning.

The NN has two inputs speed error and time. The output is the change of current i_q*. A multilayer NN with back-propagation training is used. The NN consists of a fully connected two-layer network. The input layer receives two inputs from speed error and time. The single hidden layer has 10 neurons with a tan-sigmoid activation function. The output layer has single neuron with linear activation function. Figure 2 depicts the structure of Back Propagation Neural Network (BPNN) [25].

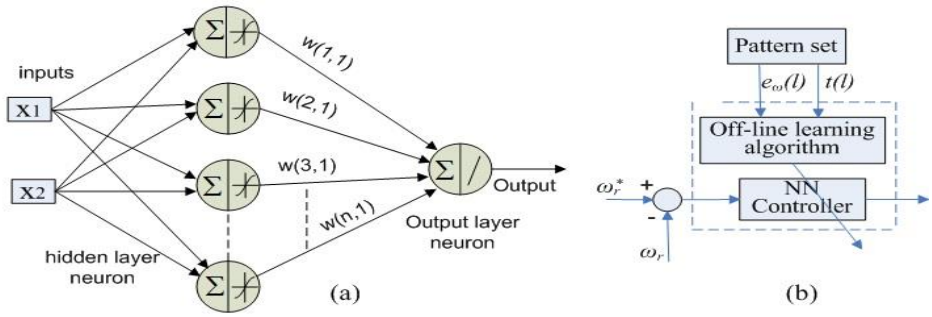

Figure 2
(a) The structure of Back Propagation Neural Network (BPNN). (b) NNC structure

3.1.3 Conventional SMC

Since the SRM is excited by DC voltage pulses through the Asymmetric Half Bridge (AHF), the sliding mode control can cope with the discrete nature of the converter. It can overcome the nonlinearities of the motor and the converter. Therefore, for the SRM assuming the load torque constant from (2):

$$\dot{\omega} = -\frac{B}{J}\omega + \frac{1}{J}T_e$$

Choosing the sliding surface: $S=\omega-\omega_{ref}$ and differentiating the sliding surface:

$$\dot{s}=\dot{\omega}_{ref}-\dot{\omega} = \dot{\omega}_{ref} + \frac{B}{J}\omega - \frac{1}{J}T_e \tag{6}$$

Stability Analysis

The following condition should be verified to force the error and its rate of change converge to the sliding surface as follows:

$$\dot{s}=\dot{\omega}_{ref}-\dot{\omega}=\dot{\omega}_{ref} + \frac{B}{J}\omega - \frac{1}{J}T_e = 0$$

Then, the torque reference which represents the equivalent control input:

$$u_{eq}=T_{eref} = B\omega + J\dot{\omega}_{ref} \tag{7}$$

To maintain the control state on the sliding surface and verify the Lyapunov stability theory, suppose this Lyapunov function: $V=0.5s^2$ and differentiating:

$$\dot{V}= s\dot{s} = s\left(\frac{B}{J}\omega - \frac{1}{J}T_e + \dot{\omega}_{ref}\right) = -sK\,sign(s) + s\left(\dot{\omega}_{ref} + \frac{B}{J}\omega - \frac{1}{J}T_e + Ksign(s)\right)$$

then, the control input : $u= B\omega + J\dot{\omega}_{ref} + JKsign(s)$

which verify (8) as follows: $\dot{V}= s\dot{s} = -sK\,sign(s) \prec 0$ provided that $K > 0$

Therefore, to assure the stability of the control input and eliminate the chattering associated with the conventional SMC, K should be large and > 0.

3.1.4 Fractional Derivative Sliding Mode Speed control

The switching function S is defined as the fractional-order nonsingular Terminal Sliding Mode (TSM) as follow [24]:

$$S = e + kD^{\lambda-1}[sign(e)^a] \tag{8}$$

Where k is a positive constant, $D^{\lambda-1}$ is fractional order derivative, λ is fractional order between $0< \lambda < 1$ and $2 > a > 1$. The derivative of (8) is:

$$\dot{S} = \dot{e} + kD^{\lambda}[sign(e)^{a}] \tag{9}$$

Substituting Eq. (6) in Eq. (9) results the following:

$$\dot{S} = \dot{e} + kD^{\lambda}\left[sign(e)^{a} \right] = \dot{\omega}_{ref} + \frac{B}{J}\omega - \frac{1}{J}T_e + kD^{\lambda}\left[sign(e)^{a} \right] \tag{10}$$

Stability Analysis

To assure the system (error and its change) constraints towards the sliding surface and reaches in finite time, the following condition should be met [22-25, 28-30]: $\dot{S} = S = 0$ and equating Eq. (10) with zero results:

$$\dot{S} = \dot{e} + kD^{\lambda}\left[sign(e)^{a} \right] = \frac{B}{J}\omega - \frac{1}{J}T_e + \dot{\omega}_{ref} + kD^{\lambda}\left[sign(e)^{a} \right] = 0$$

Resulting the equivalent control: $u_{eq} = T_{eref} = B\omega + kJD^{\lambda}\left[sign(e)^{a} \right]$

To verify the Lyapunov stability theory, this Lyapunov function should be verified $\dot{V} = \dot{S}S \prec 0$, and:

$$S\dot{S} = S\left(e + kD^{\lambda}\left[sign(e)^{a} \right] \right) \prec 0 \Rightarrow -S\left(\omega - \omega_{ref} - kD^{\lambda}\left[sign(e) \right] \right) ,$$

therefore, k should be > 0 to ensure global asymptotic stability.

3.2 Current Control

To obtain precise speed control and speed the response of the rotor speed and torque, the current loop is controlled by SMC. Fractional order SMC of current loop provides more degree of freedom in terms of faster speed and torque response. We controlled this loop by hysteresis, conventional SMC and Adaptive Fractional Order (SMC) (AFOSMC) and designed them in the following subsections:

3.2.1 Hysteresis controller

3.2.2 Conventional SMC

3.2.3 Fractional Order SMC (FOSMC)

3.2.4 Adaptive FOSMC

3.2.1 Hysteresis Controller

The hysteresis band was selected carefully as 0.5 A to obtain faster response because a high band increases the torque ripples.

3.2.2 Conventional SMC

The current loop compares the actual stator currents with reference currents from the torque reference after normalizing it. We take the sliding surface as a simple error as follows: $S = e = i_{ref} - i$, then, $\dot{S} = \dot{i}_{ref} - \dot{i} = \dot{i}_{ref} - V_n + i_n R_n + 2\frac{T}{i_n}\omega$

Stability Analysis

To guarantee the system error and its rate of change converge to the sliding surface by imposing; $S = \dot{S} = 0$, this results the control law after adding the switching law: $V_n = i_n R_n + 2\frac{T}{i_n}\omega + K sign(e)$

To guarantee the stability of the control state on the sliding surface, the Lyapunov condition should be verified as follows: $\dot{V} = \dot{S}S \prec 0$,

$\dot{V} = \dot{S}S = -K\ sign(e) \prec 0$, therefore, *K* should be large positive to guarantee the stability of the Lyapunov theory and eliminate the chattering.

3.2.3 Fractional Order SMC (FOSMC)

To achieve more degrees of freedom, we propose the following fractional order nonsingular Terminal Sliding Mode surface [24]:

$S = e + kD^{\lambda-1}[sign(e)^a]$, $0 < \lambda < 1$, *D* is the fractional order differentiator operator and *a* is a real constant between 1 and 2.

Stability Analysis

Differentiating the sliding surface, we obtain the following:

$$\dot{S} = \dot{e} + kD^{\lambda}\left[sign(e)^a \right] = \dot{i}_{ref} - V_n + i_n R_n + 2\frac{T}{i_n}\omega + kD^{\lambda}\left[sign(e)^a \right],$$

To constraint the error is moving always toward the sliding surface $S=0$ and its rate of change: $S = \dot{S} = 0$ .Then, we get the equivalent control law:

$V_n = i_n R_n + 2\frac{T}{i_n}\omega + kD^{\lambda}\left[sign(e)^a \right]$, According to the Lypunov stability theory and guarantee the stability of the control law, $\dot{V} = \dot{S}S \prec 0$

$$S\dot{S} = S\left(\dot{e} + kD^{\lambda}\left[sign(e)^a \right] \right) \prec 0 \implies -S\left(\dot{i} - \dot{i}_{ref} - kD^{\lambda}\left[sign(e)^a \right] \right) \prec 0,$$

therefore, *k* should be > 0 to guarantee the control state remaining along the sliding surface.

3.2.4 Adaptive Fractional Order SMC

This fast reaching law will be proposed in this section to obtain faster convergence time as follows [24, 25]:

$\dot{S}=-Ksign(e)^b$, $1\prec b\prec 2$ and will be added to the equivalent control as follows:

$$\dot{S}=\dot{e}+kD^{\lambda}\left[sign(e)^a \right]=\dot{i}_{ref}-V_n+i_nR_n+2\frac{T}{i_n}\omega+kD^{\lambda}\left[sign(e)^a \right]=-Ksign(S)^b=0$$

Stability Analysis

To assure maintaining the control state on the sliding surface: $\dot{V}=\dot{S}S\prec 0$

$\dot{V}=\dot{S}S=S(-Ksign(S)^b)\prec 0 \Rightarrow$ *This means that* $K\succ 0$ *for aymptotic stability.*

Then, the control input: $V_n=i_nR_n+2(T/i_n)\omega+kD^{\lambda}\left[sign(e)^a \right]+Ksign(S)^b$

3.3 Implementation of the Fractional Order Derivative

Fractional integration and differentiation can be approximated using many methods; continuous like Carlson's method, Matsuda's method, Oustaloup method and Chareff's method and discrete like the backward Euler and PSE or backward Euler and CFE or trapezoidal rule and CFE. There are three definitions to define the fractional operator in the time domain; the Grunwald- Letnikov (GL) and the Riemann-Liuville (RL) and the Caputo fractional definitions.

The Laplace transform is the best method for evaluating the fractional integrator or differentiator of zero initial conditions for the GL or RL methods (for order r) which can be defined by: $L\left\{ {}_aD_t^{\pm r} f(t);s \right\}=s^{\pm r}F(s)$

The discretization of the fractional-order operator s^{α} (α is a real number) can be described by the so-called generating function s = ω (z^{-1}). The most commonly used three discretization schemes are the trapezoidal (Tustin) rule, the backward difference (Euler) rule, and the most commonly used Al-Alaoui operator.

The generating function can be used in the following formula:

$$\omega(z^{-1})=\frac{1}{\beta T}\frac{1-z^{-1}}{\gamma+(1-\gamma)z^{-1}} \tag{11}$$

Where β and γ are the gain and phase tuning parameters, respectively. For example, when β = 1 and γ = {0, 1/2, 7/8, 1, 3/2}, the generating function (11) becomes the forward Euler, the Tustin, the Al-Alaoui, the backward Euler and the implicit Adams rules, respectively.

There are two main methods to find the digital approximation of the generating function; Power Series Expansion (PSE) and Continued Fraction Expansion (CFE). This approximated transfer function can be implemented on any processor like D.S.P. The approximation of PSE is in the form of polynomials that is the form of FIR filter which has only zeros. While the approximation of CFE is in the form of rational transfer function (IIR filter) which has poles and zeros. But approximation of rational functions converges faster than PSE and converges in larger domain in the complex plane [31].

Therefore, we adopted the discrete transfer function based on the Aouli (which is mixed of the Euler rule and the Trapezoidal rule) and CFE discretization scheme. This method has better approximation in the high frequency range than that based on the Tustin rule [32]. Therefore, the generating function for discretization will be:

$$(\omega(z^{-1}))^{\pm r} = (\frac{8}{7T}\frac{1-z^{-1}}{1+z^{-1}/7})^{\pm r} \tag{12}$$

CFE can be used to approximate the function (12) which is an infinite order of rational discrete transfer function to finite order rational one.

$$\begin{aligned}(\omega(z^{-1}))^{\pm r} &= \left(\frac{1+a}{T}\right)^{\pm r} CFE\left\{(\frac{1-z^{-1}}{1+az^{-1}})^{\pm r}\right\}_{p,q} \\ &= \left(\frac{1+a}{T}\right)^{\pm r}\frac{P_p(z^{-1})}{Q_q(z^{-1})} \\ &= \left(\frac{1+a}{T}\right)^{\pm r}\frac{p_0+p_1z^{-1}+....+p_mz^{-p}}{q_0+q_1z^{-1}+....+q_mz^{-q}}\end{aligned} \tag{13}$$

Where CFE{u} denotes the continued fraction expansion of u; p and q are the orders of the approximation and P and Q are polynomial functions of degrees p and q. Normally, we can set $p = q = n$.

The value of approximation order n is truncated to $n = 5$ and the weighting factor a was chosen = 1/3. Assume sampling period $T = 0.001$ s. For $r = 0.5$ we have the following approximation of the fractional half-order derivative [33, 34]:

$$G(z^{-1}) = \frac{985.9-1315z^{-1}+328.6z^{-2}+36.51z^{-3}}{27-18z^{-1}-3z^{-2}+z^{-3}} \tag{14}$$

4 Simulation Results

In this section, we show the effect of each loop where the controllers were simulated in each loop (speed and current) using MATLAB/SIMULINK. The proposed method AFOSMC (CL) and FOSMC (SL) will be compared to two methods. These two methods are PI (SL), HC (CL) and NNC (SL), HC (CL). The MATLAB model of the proposed system is shown in Figure 3. The simulation results proved the improved response of AFOSMC and FOSMC compared to the others in terms of lower torque and speed ripples and NNC in terms of faster speed response. The proposed method will be tested under the following effects:

4.1 Motor performance without uncertainties (inertia J=0.05)

4.2 Motor performance with mechanical parameter uncertainties 100% (inertia J=0.1)

4.3 Load torque step change

4.4 Effects of the proposed controllers on each loop at high speeds

The SRM 6/4 parameters are as follows: R_s= 0.05-ohm, Unaligned inductance= 0.67 mH, Aligned inductance= 20.3 mH, inertia coefficient (J)= 0.05 kg.m^2 and V_{dc}= 250 V.

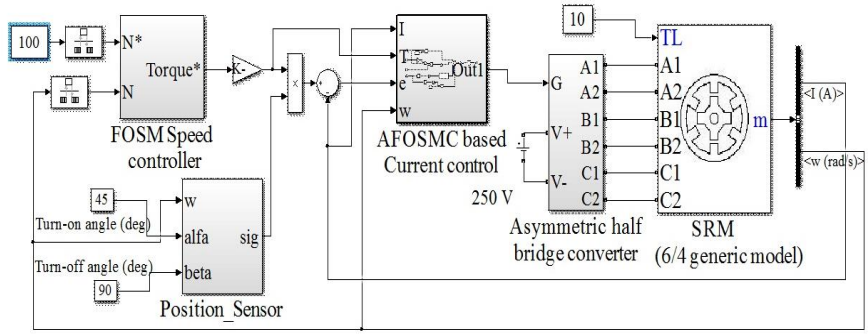

Figure 3
The MATLAB model of the proposed system

4.1 Motor Performance without Uncertainties

This test shows the performance characteristics of the motor for the proposed controllers as shown in Figures 3, 4 and 5 at load torque T_L= 10 N.m. The AFOSMC (CL) and FOSMC (SL) has better torque ripples, speed ripples and speed steady state error compared to the other controllers and better settling time

compared to PI. The NNC has better settling time compared to the others. PI has the least torque and speed overshoots as illustrated in Table 1.

Table 1

The motor performance without uncertainties of J=0.05 kg.m2

Performance characteristics	FOSMC (SL) AFOSMC (CL)	PI (SL) HC(CL)	NNC (SL) HC (CL)
Settling time	26.16 ms	27.4 ms	16.34 ms
Torque ripples	10.8 %	30.4 %	31 %
Torque overshoot	314 N.m	217.6 N.m	405 N.m
Speed ripples	0.064 rpm	0.23 rpm	0.22 rpm
Speed overshoot	778.6 rpm	0	0
Speed steady state error	0.2 rpm	1.4 rpm	1.4 rpm

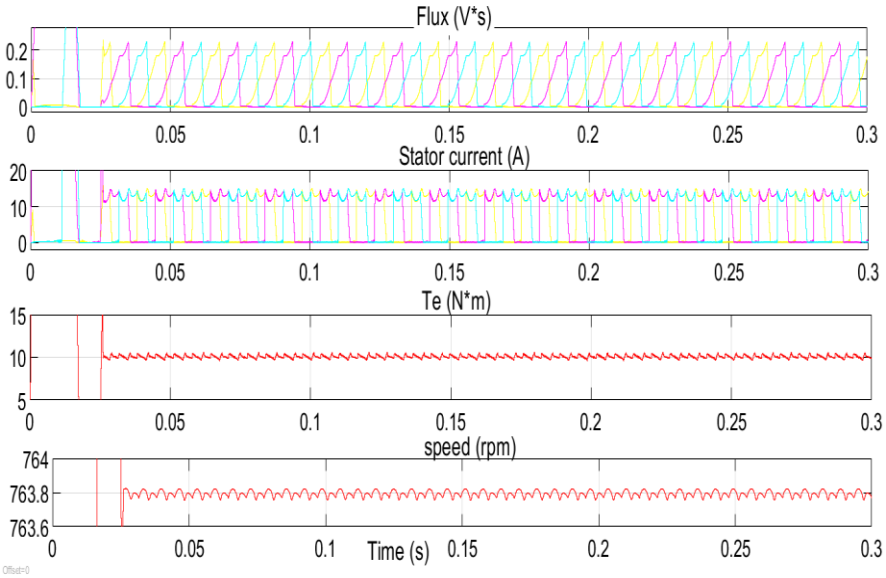

Figure 4

The motor performance of AFOSMC without uncertainties (J=0.05)

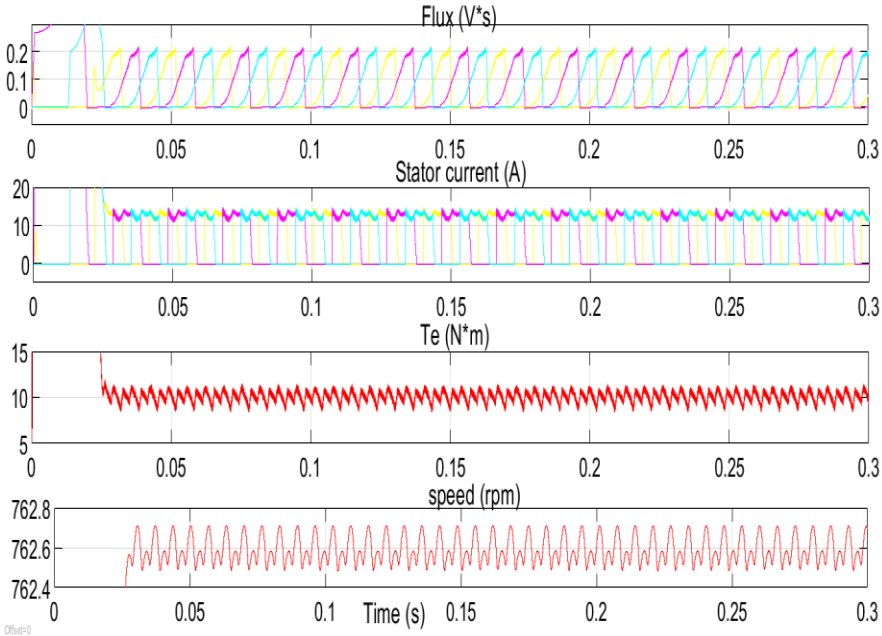

Figure 5
The motor performance of PI (SL) and HC (CL) without uncert. (J=0.05)

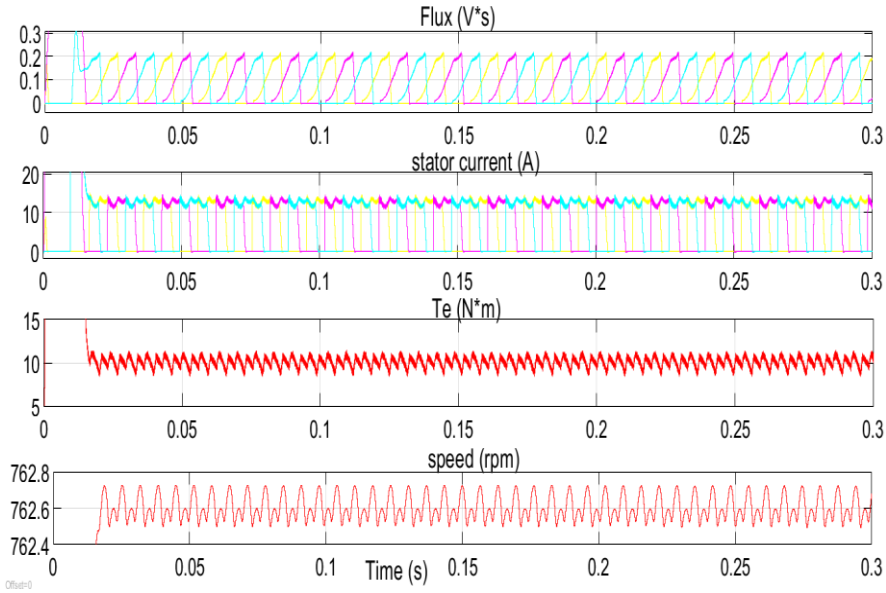

Figure 6
The motor performance of NNC (SL) AND HC (CL) without uncert. (J=0.05)

4.2 Motor Performance with 100% Uncertainties of Inertia J

This test shows the performance characteristics of the motor for the proposed controllers with uncertainties of the rotor inertia 100% as shown in Figures 7, 8 and 9. The AFOSMC has better torque ripples, speed ripples and speed steady state error compared to the other controllers and better settling time compared to PI. The other controllers PI and NNC have rather improved response for the other characteristics as for normal operation without uncertainties. Therefore, from Table 2, the proposed controllers AFOSMC (CL) and FOSMC (SL) achieved its target of minimization of the torque and speed ripples which are inherent disadvantages of SRM.

Table 2

The motor performance with inertia uncertainties 100 % of J=0.1 kg.m^2

Performance characteristics	FOSMC (SL) AFOSMC (CL)	PI (SL) HC(CL)	NNC (SL) HC (CL)
Settling time	35.3 ms	52.2 ms	31.19
Torque ripples	15.6%	35.1%	35.5%
Torque overshoot	314 N.m	217.6 N.m	405 N.m
Speed ripples	0.07 rpm	0.14 rpm	0.15 rpm
Speed overshoot	2 rpm	0	0
Speed steady state error	0.2 rpm	1.4 rpm	1.4 rpm

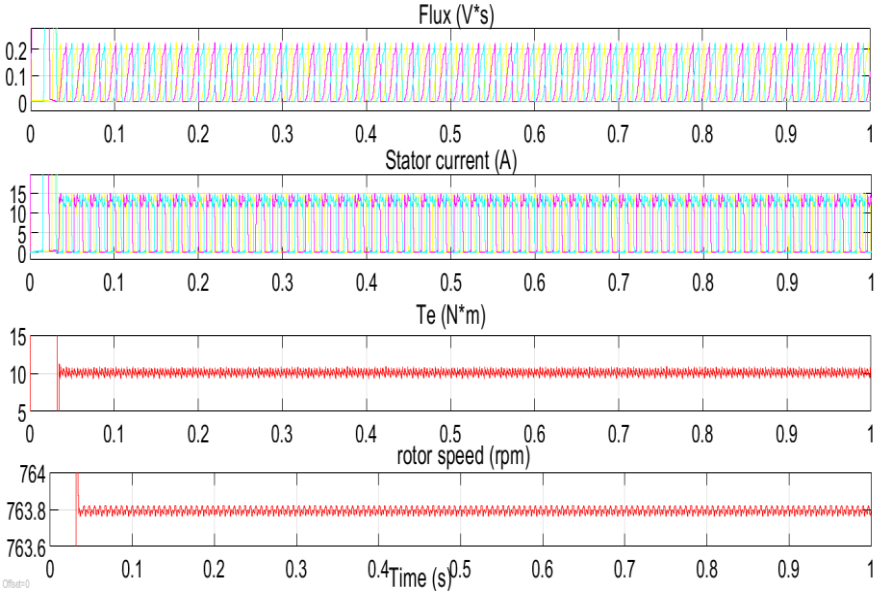

Figure 7

The motor performance of FOSMC (SL) and AFOSMC (CL) with uncert. 100% (J=0.1)

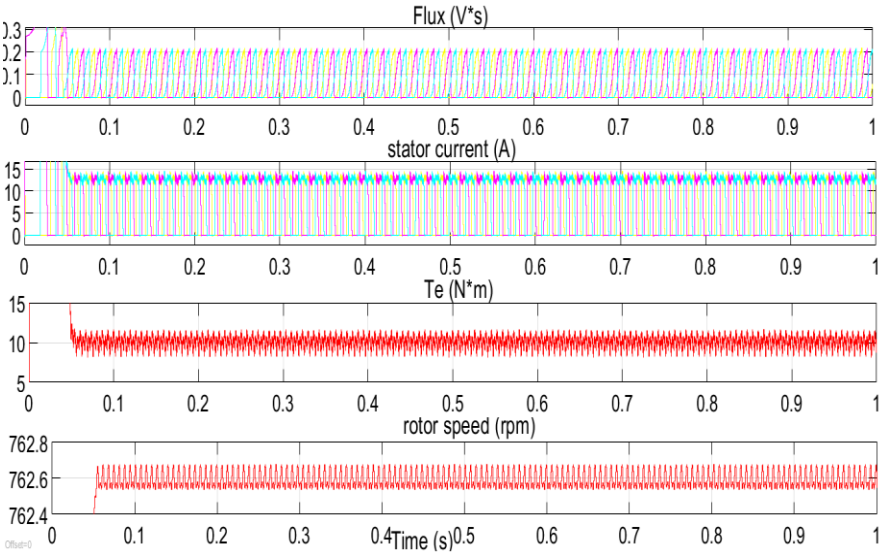

Figure 8
The motor performance of PI (SL) and HC (CL) with uncert. 100 % (J=0.1)

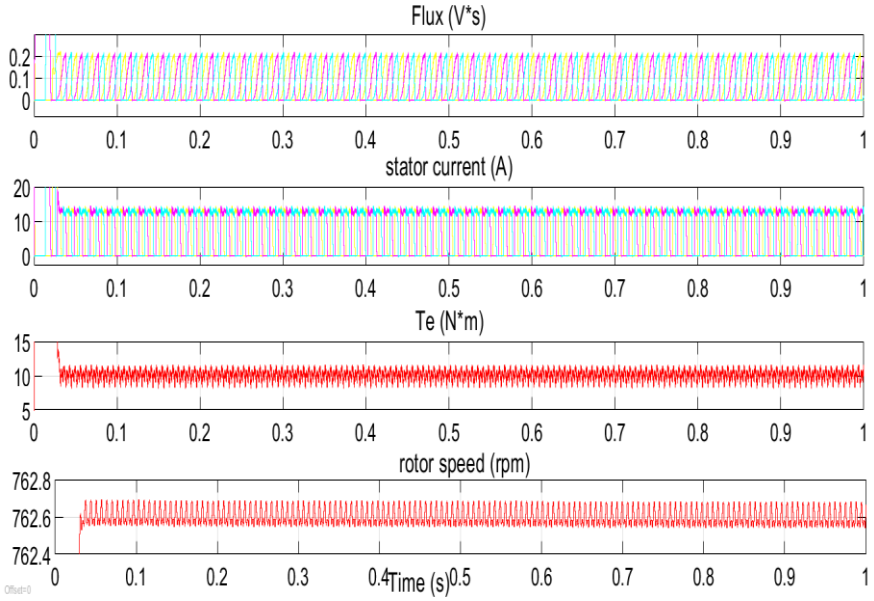

Figure 9
The motor performance of NNC (SL) and HC (CL) with uncert. 100% (J=0.1)

4.3 Load Torque Step Change

In this test, we increased the load torque (T_L) from 5 N.m to 10 N.m at t=0.2 and the total load were removed suddenly at t= 0.5. From Figures 10-12, at T_L =5 N.m, the torque ripples percentage ratios are 12%, 39.2% and 40% for the three controllers AFOSMC, PI and NNC respectively. Also, the speed errors ratios are 0.004%, 0.013% and 0.22%.

At T_L =10 N.m, the torque ripples percentage ratios for the three controllers AFOSMC, PI and NNC are 10.8%, 30.4% and 31% respectively. The speed errors for them are 0.009%, 0.03% and 0.196% respectively. Therefore, from Figures 10, 11 and 12, the proposed controller AFOSMC has the least torque ripples and speed errors compared to the other controllers against external load torque disturbance. In addition, the proposed controller has faster step torque response than the other controllers as shown in Figures 13 and 14.

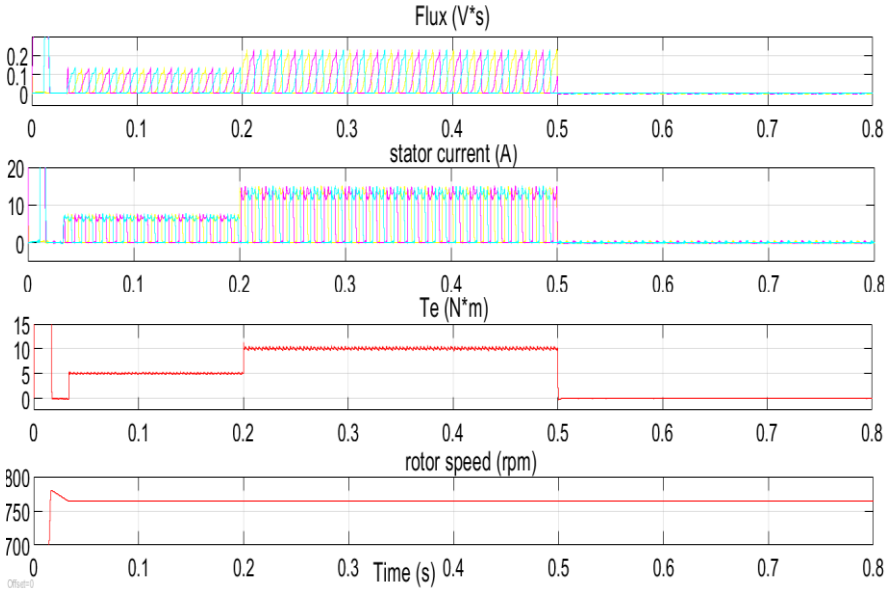

Figure 10
The motor performance of step load change for AFOSMC

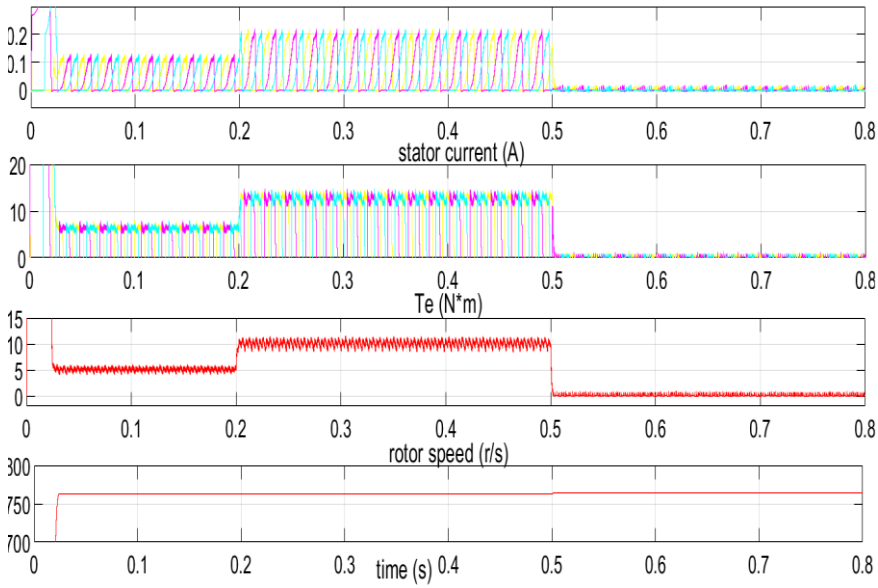

Figure 11
The motor performance of step load change for PI

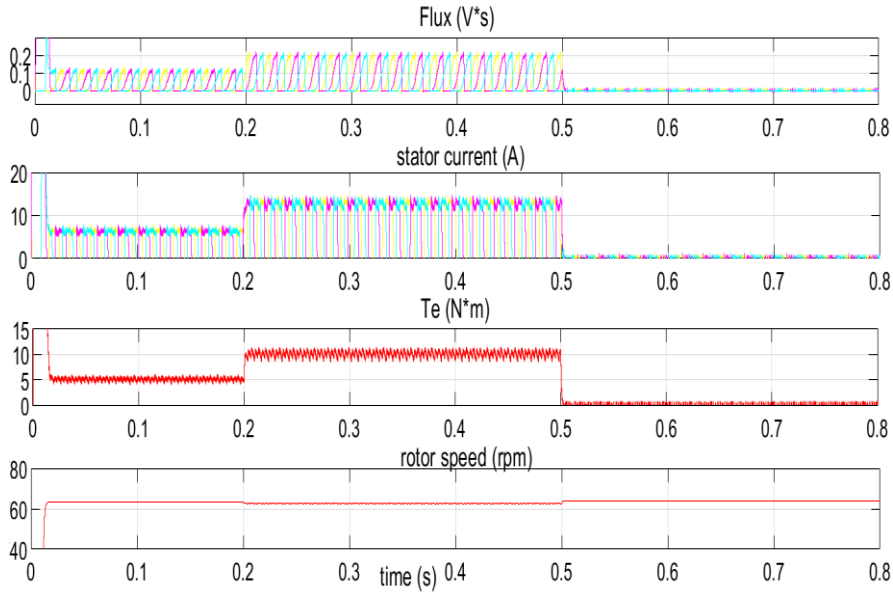

Figure 12
The motor performance of step load change for NNC

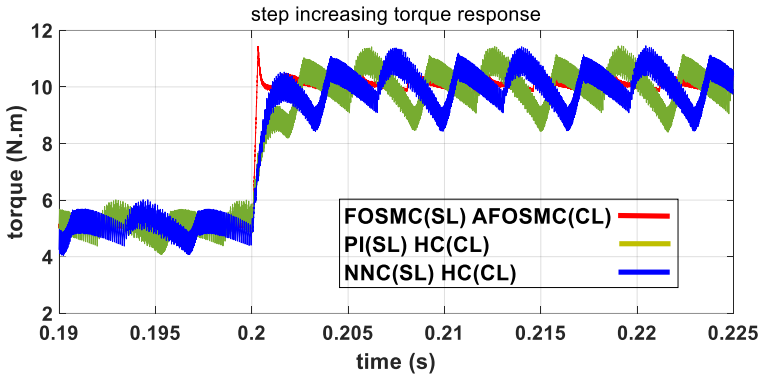

Figure 13

The step increasing load response for the three controllers' schemes

4.4 Effects of Controllers on Each Loop at High Speeds

In this test, the different sliding mode controllers controlled the two loops to show its effect and the effects of the fractional order SMC and AFOSMC for different inertia (J= 0.05 and 0.008). In this test, the fractional order differentiator was taken as λ=0.1. Figures 15-16, show the current loop (CL) with AFOSMC and speed loop (SL) with FOSMC has the fastest speed response where the conventional SMC has longer settling time especially at higher speeds.

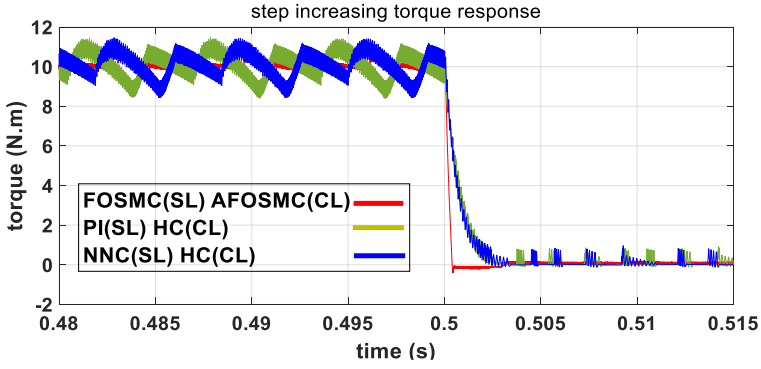

Figure 14

The step decreasing load response for the three controllers' schemes

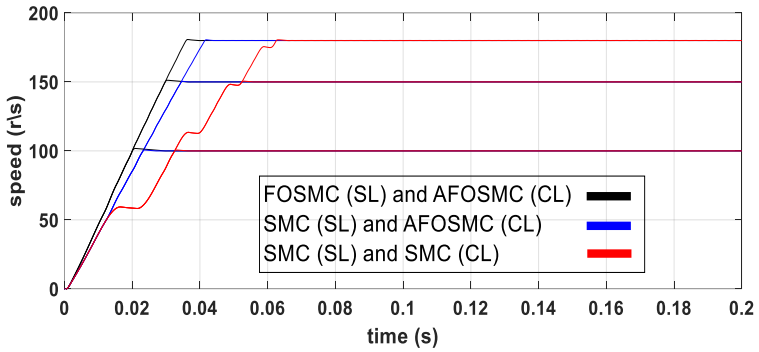

Figure 15

The speed response of speed and current loops at J=0.05 with λ= 0.1

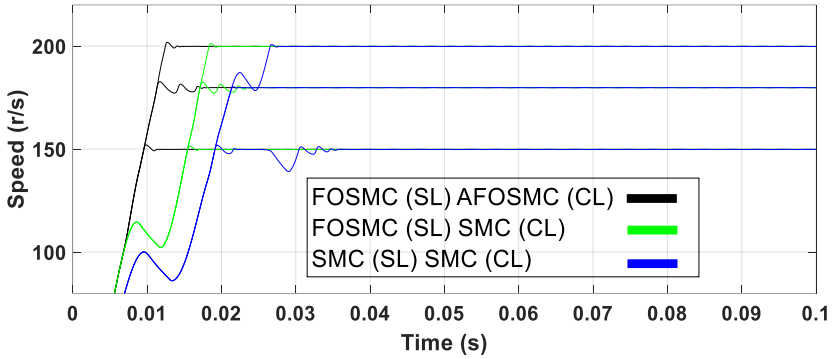

Figure 16

The speed response of speed and current loops at J=0.008 with λ= 0.1

Conclusions

The proposed controller AFOSMC, achieved its target, by compensating for the inherent disadvantages of SRM, which are torque/speed ripples and steady state errors. The results were validated by comparing them with NNC, HC and PI in the two loops of the closed loop control of SRM. The proposed controller provided the desired improved response of lower torque and speed ripples, during normal operation and under the effect of mechanical parameter J (rotor inertia) variation at 100-%. In addition, the proposed controller exhibited a faster speed and torque response, compared to conventional sliding mode control, NNC, HC and PI at high speeds for different inertia.

References

[1] Ahmad Reda, Ahmed Bouzid, József Vásárhelyi, “Model predictive control for automated vehicle steering”, Acta Polytechnica Hungarica, Vol. 17, No. 7, 2020, pp. 163-182

[2] Emil PRECUP, Raul-Cristian ROMAN, Teodor-Adrian TEBAN, Adriana ALBU, Emil M. PETRIU and Claudiu POZNA, "Model-free control of finger dynamics in prosthetic hand myoelectric-based control systems", Studies in Informatics and Control, Vol. 29, No. 4, pp. 399-410, 2020

[3] A. S. Oshaba, E. S. Ali, S. M. Abd-Elazim, "PI controller design for MPPT of photovoltaic system supplying SRM via BAT search algorithm", Neural Computing and Applications, Vol. 28, No. 4, 2017, pp. 651-667

[4] A. S. Oshaba, E. S. Ali, S. M. Abd-Elazim, "ACO based speed control of SRM fed by photovoltaic system", Int. J Electr Power Energy Syst., Vol. 67, 2015, pp. 529-536

[5] R. Kalai Selvi, R. Suja Mani Malar, "A bridgeless Luo converter based speed control of switched reluctance motor using Particle Swarm Optimization (PSO) tuned Proportional Integral (PI) controller", Microprocessors and Microsystems, Vol. 75, 2020, pp. 1-9

[6] Jia-Jun Wang, "Parameter optimization and speed control of switched reluctance motor based on evolutionary computation methods", Swarm and Evolutionary Computation Vol. 39, 2018, pp. 86-98

[7] Chwan-Lu Tseng, Shun-Yuan Wang, Shao-Chuan Chien and Chaur-Yang Chang, "Development of a Self-Tuning TSK-Fuzzy speed control strategy for switched reluctance motor", IEEE Transactions on Power Electronics, Vol. 27, No. 4, April 2012, pp. 2141-2152

[8] Kohei Aiso; Kan Akatsu, "High speed SRM using vector control for electric vehicle", IEEE CES Transactions on Electrical Machines and Systems, Vol. 4, No. 1, March 2020, pp. 61-68

[9] Abdulrahman J. Babqi and Basem Alamri, "A Comprehensive comparison between finite control set model predictive control and classical proportional-integral control for grid-tied power electronics devices", Acta Polytechnica Hungarica Vol. 18, No. 7, 2021, pp. 67-87

[10] Fahad Al-Amyal, Mahmoud Hamouda and László Számel, "Torque quality improvement of switched reluctance motor using Ant Colony algorithm", Acta Polytechnica Hungarica Vol. 18, No. 7, 2021, pp. 129-150

[11] Radu-Emil Precup, Stefan Preitl and Gabriel Faur, "PI predictive fuzzy controllers for electrical drive speed control: methods and software for stable development", Computers in Industry, Vol. 52, No. 3, 2003, pp. 253-270

[12] Radu-Emil Precup and Stefan Preitl, "Optimisation criteria in development of fuzzy controllers with dynamics", Engineering Applications of Artificial Intelligence, Vol. 17, No. 6, 2004, pp. 661-674

[13] Serkan Sezen, Ercument Karakas, Kadir Yilmaz and Murat Ayaz, "Finite element modeling and control of a high-power SRM for hybrid electric

vehicle", Simulation Modelling Practice and Theory, Vol. 62, 2016, pp. 49-67

[14] Changliang Xia, Ziran Chen and Mei Xue, "Adaptive PWM speed control for switched reluctance motors based on RBF neural network", IEEE 2006 6th World Congress on Intelligent Control and Automation

[15] Linhao Sheng, Guofeng Wang and Yunsheng Fan, "Adaptive second-order global terminal sliding mode direct torque control of switched reluctance motor based on RBFNN", 2020 39th Chinese Control Conference (CCC), 27-29 July 2020

[16] Yong-Chao Liu, Salah Laghrouche, Abdoul N'Diaye and Maurizio Cirrincione, "Hermite neural network-based second-order sliding-mode control of synchronous reluctance motor drive systems", Journal of the Franklin Institute, Vol. 358, 2021, pp. 400-427

[17] Chih-Hong Lin and S. J. Chiang, "Torque-ripple reduction in switched reluctance motor drive using SHRFNN control", IEEE 2006 37th IEEE Power Electronics Specialists Conference (PESC 2006)

[18] Mohammad Divandari, Behrooz Rezaie and Abolfazl Ranjbar Noei, "Speed control of switched reluctance motor via fuzzy fast terminal sliding-mode control", Computers and Electrical Engineering, Vol. 80, 2019, pp. 1-16

[19] Jia-JunWang, "A common sharing method for current and flux-linkage control of switched reluctance motor", Electric Power Systems Research, Vol. 131, February 2016, pp. 19-30

[20] Xiaodong Sun, Liyun Feng, Kaikai Diao and Zebin Yang, "An improved direct instantaneous torque control based on adaptive terminal sliding mode for a segmented-rotor SRM", IEEE Transactions on Industrial Electronics, Vol. 68, No. 11, 2021, pp. 10569-10579

[21] Xuedong Sun, Jiangling Wu, Gang Lei, Youguang Guo and Jianguo Zhu, "Torque ripple reduction of SRM drive using improved direct torque control with sliding mode controller and observer", IEEE Transactions on Industrial Electronics, Vol. 68, No. 10, 2021, pp. 9334-9345

[22] D. Jiang, W. Yu, J. Wang, Y. Zhao, Y. Li and Y. Lu, "A speed disturbance control method based on sliding mode control of permanent magnet synchronous linear motor. IEEE Access, Vol. 7, 2019, pp. 82424-82433

[23] Dhafer J. Almakhles, "Robust backstepping sliding mode control for a quadrotor trajectory tracking application", IEEE Access, Vol. 8, 2020, pp. 5515-5525

[24] Ashraf Hagras, Abdelnasser Nafeh, "Model free fractional order sliding mode control of permanent magnet synchronous motor", International Journal of Modeling, Identification and Control, Accepted (In production)

[25] Ashraf Hagras, "Performance comparison of NN and fractional order SM sensorless speed control of IPMSM drive", Journal of Electrical Engineering (JEE-POLITEHNICA Publishing House), Accepted

[26] Arjon Turnip and Jonny H. Panggabea, "Hybrid controller design based magneto-rheological damper lookup table for quarter car suspension", International Journal of Artificial Intelligence, Vol. 18, No. 1, 2020, pp. 193-206

[27] Raul-Cristian Roman, Radu-Emil Precup and Emil M. Petriu, "Hybrid data-driven fuzzy active disturbance rejection control for tower crane systems", European Journal of Control, Vol. 58, 2021, pp. 373-387

[28] J.-J. E. Slotine and W. Li, "Applied Nonlinear Control", Prentice Hall International Inc. (1991)

[29] S. Sastry and M. Bodson, "Adaptive Control Stability, Convergence and Robustness", Engle Wood Cliffs, Newjersy, 1989

[30] M. Krstic, Ioannis Kandlakopoulos and Peter Kokotonic, "Nonlinear and Adaptive Control Design", John Wiley&Sons, Inc.

[31] Y. Q. Chen and B. M. Vinagre, "A new IIR-type digital fractional order differentiator", Signal Processing, Vol. 83, No. 11, 2003, pp. 2359-2365

[32] Y. Q. Chen and K. L. Moore, "Discretization schemes for fractional-order differentiators and integrators", IEEE Transactions on Circuits and Systems -I: Fundamental Theory and Applications, Vol. 49, No. 3, 2002, pp. 363-367

[33] I. Petras, "Fractional order feedback control of a DC motor", Journal of Electrical Engineering, Vol. 60, No. 3, 2003, pp. 117-128

[34] Andrzej Ruszewski, Andrzej Sobolewski, "Position control of DC motor using fractional order controller", Archives of Electrical Engineering, Vol. 62, No. 3, 2013, pp. 505-516